

A Critical Look at Cosmological Perturbation Theory Techniques

Jordan Carlson*

Department of Physics, 366 LeConte Hall, University of California Berkeley, CA 94720

Martin White†

Departments of Physics and Astronomy, 601 Campbell Hall, University of California Berkeley, CA 94720

Nikhil Padmanabhan‡

Physics Division, Lawrence Berkeley National Laboratory, 1 Cyclotron Rd., Berkeley, CA 94720

Recently a number of analytic prescriptions for computing the non-linear matter power spectrum have appeared in the literature. These typically involve resummation or closure prescriptions which do not have a rigorous error control, thus they must be compared with numerical simulations to assess their range of validity. We present a direct side-by-side comparison of several of these analytic approaches, using a suite of high-resolution N-body simulations as a reference, and discuss some general trends. All of the analytic results correctly predict the behavior of the power spectrum at the onset of non-linearity, and improve upon a pure linear theory description at very large scales. All of these theories fail at sufficiently small scales. At low redshift the dynamic range in scale where perturbation theory is both relevant and reliable can be quite small. We also compute for the first time the 2-loop contribution to standard perturbation theory for CDM models, finding improved agreement with simulations at large redshift. At low redshifts however the 2-loop term is larger than the 1-loop term on quasi-linear scales, indicating a breakdown of the perturbation expansion. Finally, we comment on possible implications of our results for future studies.

PACS numbers:

I. INTRODUCTION

The character and evolution of the large-scale structure of the Universe has been the subject of much research in recent decades. As it is currently understood, large-scale structure grows through a process of gravitational instability starting from a nearly scale-invariant spectrum of Gaussian fluctuations at early times. On very large scales the matter distribution of our universe today is well modeled by linear perturbation theory. On scales below about 10 Mpc, on the other hand, the dynamics are highly non-linear and we must resort to direct numerical simulations of the N-body problem to understand the clustering of matter or its tracers.

On intermediate, or quasi-linear, scales there is the possibility that the matter distribution may be modeled analytically by extending perturbation theory beyond linear order. This possibility has received renewed attention recently due to the interest in using baryon acoustic oscillations as a probe of the expansion history of the Universe and of the nature of dark energy [1]. Since the baryonic features are at large scales ($\mathcal{O}(100)$ Mpc) it is plausible that higher order perturbation theory could model subtle corrections to the linear result with some accuracy. More generally, investigation of perturbation theory may allow some improvement in theoretical pre-

dictions for the next generation of very large surveys.

Consequently, a number of new ideas have been introduced in recent years for computing statistical properties of the matter distribution, most importantly the 2-point function or power spectrum. Regrettably these approaches involve uncontrolled approximations, providing no simple way of estimating the theoretical uncertainty. Since perturbation theory is expected to fail on sufficiently small scales, the domain of validity of any particular approach is therefore unclear, and the only known way to test their accuracy is to compare their predictions with the results of N-body simulations. In the past this has been done on a case-by-case basis, with one theory tested for one cosmology against one suite of N-body simulations, focusing primarily on the power spectrum. Recently there have been some attempts to compare multiple theories simultaneously [2, 3], or to examine statistics other than the power spectrum [4, 5, 6]. However a comprehensive comparison has been lacking, and with the recent proliferation of analytic techniques it is natural to ask how well these theories actually perform. With near-future observations potentially depending on these techniques and with recent advances in N-body algorithms and computing power, it is timely to revisit this issue.

In this paper we present a direct comparison of several recent analytic predictions for the clustering of matter on quasi-linear scales. We restrict our attention to the matter fluctuations, because very few of the existing treatments can handle biased tracers such as dark matter halos and galaxies. We use modern, high-resolution N-body simulations as our reference points, which provide

*Electronic address: jwgcarlson@berkeley.edu

†Electronic address: mwhite@berkeley.edu

‡Electronic address: NPadmanabhan@lbl.gov

highly accurate [7, 8, 9] (though computationally expensive) estimates for statistical observables of the matter distribution. By comparing the analytic predictions for two cosmologies, one close to the current best-fit model and one more extreme, we are able to judge the relative merits of each approach.

The paper is organized as follows. In Section II we start by reviewing the dynamical equations that govern the evolution of the matter distribution and discuss the relevant statistical quantities that one may compute. We then continue by summarizing the different analytic approaches we consider in this paper. In Section III we describe the N-body simulations that are used as a reference point for the comparison. In Section IV we plot the various approaches together, discuss qualitatively how well they agree with simulations, and propose several ways to quantify this agreement. We discuss the results of this comparison in Section V, and make some closing remarks in Section VI.

II. ANALYTIC METHODS

We start by reviewing the different analytic methods we consider - our goal is not to provide a comprehensive description of each method, but to provide an overview and highlight the relationships between the different methods.

A. Dynamics and Linear Theory

By far the most popular approach to an analytic description of large-scale structure is to approximate the matter distribution as an irrotational fluid, characterized by a density contrast $\delta(\mathbf{x}) = \rho(\mathbf{x})/\bar{\rho} - 1$ and a peculiar velocity divergence $\theta(\mathbf{x}) = \nabla \cdot \mathbf{v}(\mathbf{x})$. The fluid equations, in Fourier space, are then (see Appendix A for a detailed derivation),

$$\frac{\partial \delta(\mathbf{k})}{\partial \tau} + \theta(\mathbf{k}) = - \int \frac{d^3 q}{(2\pi)^3} \frac{\mathbf{k} \cdot \mathbf{q}}{q^2} \theta(\mathbf{q}) \delta(\mathbf{k} - \mathbf{q}), \quad (1a)$$

$$\frac{\partial \theta(\mathbf{k})}{\partial \tau} + \mathcal{H} \theta(\mathbf{k}) + \frac{3}{2} \Omega_m \mathcal{H}^2 \delta(\mathbf{k}) = - \int \frac{d^3 q}{(2\pi)^3} \frac{k^2 \mathbf{q} \cdot (\mathbf{k} - \mathbf{q})}{2q^2 |\mathbf{k} - \mathbf{q}|^2} \theta(\mathbf{q}) \theta(\mathbf{k} - \mathbf{q}). \quad (1b)$$

Here $d\tau = dt/a(t)$ is conformal time, $\Omega_m(\tau) = \bar{\rho}(\tau)/\rho_{\text{crit}}(\tau)$, and $\mathcal{H} = aH$ is the conformal Hubble parameter. (Note that we adopt the Fourier transform convention that puts the $(2\pi)^3$ in the wavevector integral. We also omit the tilde that is usually used to decorate Fourier space quantities.) The non-linear nature of these equations is manifest in the mode-coupling integrals.

Working to linear order in δ and θ , we obtain

$$\delta_L(\mathbf{k}; z) = \frac{D(z)}{D(z_i)} \delta_i(\mathbf{k}) \quad (2)$$

and

$$\theta_L(\mathbf{k}; z) = -\mathcal{H}(z) f(z) \frac{D(z)}{D(z_i)} \delta_i(\mathbf{k}), \quad (3)$$

where δ_i is the density contrast at some early time z_i when linear theory is certainly valid, D is the linear growth function (normalized to 1 at $z = 0$), and $f \equiv d \ln D / d \ln a$. At early times $\Omega_m \approx 1$ and $D \propto a$. For convenience we define δ_0 to be the linear density contrast today, i.e. $\delta_0(\mathbf{k}) = \delta_L(\mathbf{k}; z = 0)$. When convenient we also follow common practice and use $\eta = \ln D$ as a time variable; for brevity we often suppress the time dependence of quantities altogether. It is further convenient to group δ and θ into a 2-component vector, $\Phi_a(\mathbf{k}) = (\delta(\mathbf{k}), -\theta(\mathbf{k})/\mathcal{H}f)$ which is proportional to $(1, 1)$ in linear theory.

B. Statistical observables

Inflation predicts, and observations have confirmed, that the initial fluctuations are predominantly adiabatic [10], almost scale-invariant [10], and very close to Gaussian [11]. Under the assumption that the initial field is Gaussian all expectation values of moments of the evolved density and velocity fields can be expressed as integrals over the linear theory power spectrum. For example, the evolved 2-point function

$$(2\pi)^3 \delta_D(\mathbf{k} + \mathbf{k}') P_{ab}(k) = \langle \Phi_a(\mathbf{k}) \Phi_b(\mathbf{k}') \rangle, \quad (4)$$

whose components are all equal to $P_L(k)$ in linear theory, can be expressed as integrals over n powers of P_L in n^{th} order perturbation theory (e.g. Eq. (A20)).

In general, to give a complete statistical description of the matter distribution at a given time, one would need to specify the entire hierarchy of connected n -point correlators. For initially Gaussian fields which are close to linear, the higher order connection functions are small and have been compared to simulations in [12]. We shall confine our attention to the 2-point function in this paper.

The non-linear propagator ([13, 14]; also known as the response function [4]) measures the correlation between the evolved field $\Phi_a(\mathbf{k}; \eta)$ and the initial conditions $\Phi_a(\mathbf{k}; \eta_i)$. It is formally defined as a functional deriva-

tive,

$$\delta_D(\mathbf{k} - \mathbf{k}')G_{ab}(k; \eta, \eta_i) = \left\langle \frac{\delta\Phi_a(\mathbf{k}; \eta)}{\delta\Phi_b(\mathbf{k}'; \eta_i)} \right\rangle, \quad (5)$$

though its significance is easier to understand from the relation

$$\langle \Phi_a(\mathbf{k}; \eta)\Phi_b(\mathbf{k}'; \eta_i) \rangle = G_{ac}(k; \eta, \eta_i) \langle \Phi_c(\mathbf{k}; \eta_i)\Phi_b(\mathbf{k}'; \eta_i) \rangle, \quad (6)$$

which we shall take as a definition henceforth. At early times or at large scales there is near-perfect correlation ($G_{ab} \approx 1$), but $G_{ab} \rightarrow 0$ on small scales as non-linear evolution washes out the initial conditions.

Because we will make reference to it later, we also introduce here the quantity

$$\Sigma^2 \equiv \frac{1}{3\pi^2} \int_0^\infty dq P_L(q), \quad (7)$$

which characterizes the scale at which non-linearities become important. In the Lagrangian formalism (see below) Σ^2 gives the variance of each component of the linear (or Zel'dovich) displacement.

C. Beyond Linear Theory

The program is now to compute the statistics of the evolved density field in terms of the initial density field. This is simple in principle but difficult in practice, because the equations of motion are both non-linear and non-local (in both configuration space and Fourier space). Non-linearity forces one to seek a perturbative solution, since exact solutions to Eqs. (1) (even if they could be found) could not be combined to construct a realistic solution. A straightforward perturbative approach is hampered by computational costs, as non-locality implies that higher order terms involve mode-coupling integrals of ever higher dimension.

This situation has prompted a study of higher-order methods for statistical observables like the power spectrum. Many of these methods were borrowed from other areas of physics (notably particle physics and fluid mechanics [15]) where they achieved mixed success. We review these below, highlighting the relationships between the different methods; the methods we consider are summarized in Table II.

The most straightforward approach is to define a series solution to the fluid equations in powers of the initial density field δ_i (or equivalently, the linearly evolved density field, δ_0). This is the basis behind **standard perturbation theory** (hereafter **SPT**; [16, 17, 18, 19, 20, 21]); a detailed description (including explicit expressions for P_{ab} to third order in P_L) is presented in the Appendix.

Comparisons with simulations (including those presented below) have shown that the domain of applicability of second order (in P_L) perturbation theory is rather small at $z \approx 0$. Furthermore, as we show below, going to

third order is not guaranteed to improve agreement, leading one to question the convergence properties of such a series expansion. If one could carry out any expansion to infinite order it would (trivially) give the correct answer. This however is usually not possible. This has led various authors to investigate ways of summing subsets of the terms to arbitrary order in some expansion coefficient.

Renormalized perturbation theory (hereafter **RPT**, see [13, 14, 22]) is a variant of Dyson-Wyld resummation (see [15] for a discussion in the context of hydrodynamics) and attempts to reorganize the perturbation expansion in terms of the non-linear propagator and non-linear vertex to improve convergence. In particular, if the vertex is approximated by its tree-level form then the power spectrum can be written as an expansion in the non-linear propagator. The resulting series is therefore no longer an expansion in powers of the initial density contrast, but rather “an expansion in orders of the complexity of the interaction” [23].

In [14] the dominant contributions to the non-linear propagator are identified and summed explicitly in the high- k limit, giving $G_{ab} \sim e^{-\Sigma^2 k^2/4}$ for large k . Matching this behavior with the 1-loop propagator (valid at low k) gives a non-perturbative prediction for G_{ab} . Substituting this propagator in the first few diagrams of the reorganized expansion then gives a non-perturbative prediction for the power spectrum [22]. We implemented the 1-loop and 2-loop mode-coupling contributions as described in [22].

The above methods work at the level of the density and velocity fields; an alternative approach is to use the fluid equations to derive equations of motion for the power spectrum and higher order correlators directly. Such an approach results in an infinite hierarchy of equations, which must be somehow truncated. The **closure theory** approach [2] does so by approximating the 3-point correlator $\langle \Phi_a \Phi_b \Phi_c \rangle$ by its leading order expression in SPT. As in [14], G_{ab} can be computed explicitly in the low- k and high- k limits, and matched naturally in intermediate regimes. The power spectrum is then obtained order-by-order via a Born-like series expansion.

A variant of this approach (hereafter **Time-RG theory** [24]) assumes a vanishing trispectrum to truncate the hierarchy. The resulting equations of motion for the power spectrum P_{ab} and bispectrum B_{abc} can then be numerically integrated forward in time, starting at some sufficiently early redshift z_i (where $P = P_L$ and $B = 0$). Since the time evolution is performed numerically, the method also allows the proper treatment of models where the linear growth factor is scale-dependent (e.g. models with quintessence or massive neutrinos [25]). This approach may be seen as a generalization of the **renormalization group perturbation theory** (hereafter **RGPT**) of [26], which is an attempt to regulate the relative divergence of 1-loop SPT using renormalization group methods.

In [27, 28, 29] a path-integral formulation of the Vlasov equation is developed in terms of the distribution func-

tion $f(\mathbf{x}, \mathbf{p}, t)$. In [30] a similar technique is applied to the fluid equations (Eq. (A10)). The key insight here is that statistical observables like the power spectrum may be obtained by taking functional derivatives of an appropriately constructed path integral (the generating functional). Straightforward perturbative evaluation of the generating functional reproduces the results of SPT, whereas applying large- N expansion techniques and truncating at fixed order in $1/N$ leads to approximations for the power spectrum and propagator. These approximate solutions agree with SPT up to a fixed order in P_0 , but also include non-perturbative contributions corresponding to infinite partial resummations of the standard expansion. We focus attention on the steepest-descent method of [30] (hereafter **Large-N**), as it is considerably easier to implement than the 2PI effective action method.

Lagrangian resummation theory [31, 32] is an extension of the well-developed Lagrangian perturbation theory. Lagrangian perturbation theory (hereafter LPT; see [33, 34, 35]) has received less attention recently than its Eulerian counterpart as a method for investigating non-linear structure growth, partly because the Lagrangian picture breaks down once shell-crossing occurs. However, recent work [31] has demonstrated that Lagrangian perturbation theory not only reproduces the SPT power spectrum at the lowest non-trivial order, but with a slight modification also yields a non-perturbative prediction for the power spectrum that corresponds to resumming an infinite set of terms in the standard expansion. We review LPT and the cumulant expansion in Appendix B.

III. SIMULATIONS

In order to assess how well the perturbative expansions are doing, we need a reference for any given cosmology. We use a new set of large dynamic range N-body simulations well suited to this purpose. These computer programs simulate the same basic physical system (a collisionless matter ‘fluid’ interacting only through gravity) that the perturbative methods attempt to describe; hence the results of the two methods, though arrived at very differently, are directly comparable.

We have elected to investigate several different cosmologies, in an attempt to better identify where and why various analytic techniques succeed and/or fail. For simplicity we consider only flat models in the CDM family. We will highlight two: the first in which a cosmological constant dominates the late-time evolution and which is close to the best-fit cosmology (Λ CDM: $\Omega_M = 0.25$, $\Omega_b h^2 = 0.0224$, $h = 0.72$, $n = 0.97$ and $\sigma_8 = 0.8$) and an extreme model (c CDM: $\Omega_M = 1$, $\Omega_b h^2 = 0.1$, $h = 0.5$, $n = 1$, $\sigma_8 = 1$) with a critical density in matter and a larger present-day normalization which emphasizes the effects of non-linearity and the erasure of baryon acoustic oscillations through mode coupling.

k	$\Delta_L^2(z=1)$		$\Delta_L^2(z=0)$	
	Λ CDM	c CDM	Λ CDM	c CDM
0.05	0.03	0.03	0.09	0.14
0.10	0.11	0.09	0.27	0.36
0.15	0.19	0.22	0.49	0.90
0.20	0.29	0.27	0.72	1.07
0.25	0.37	0.38	0.94	1.51

TABLE I: The value of the dimensionless, linear power spectrum at $z = 1$ and $z = 0$ at several fiducial wavenumbers for our two example cosmologies. k is given in $h \text{ Mpc}^{-1}$.

For each cosmology the transfer function, $T(k)$, was computed by evolving the coupled Boltzmann, fluid, and Einstein equations using the publicly available package CAMB (<http://www.camb.info>). The resulting power spectra were then used both as input to the perturbative methods and to generate initial conditions for the N-body simulations (Table I gives the amplitude of the dimensionless power at some fiducial wavenumbers).

A number of numerical issues need to be addressed in order to ensure that our simulations provide an adequate reference. Our workhorse simulations each employ 1024^3 equal mass dark matter particles in a periodic, cubical box of side length $2 h^{-1} \text{ Gpc}$. By employing such large volumes we are highly insensitive to the periodicity of the box, which represents a fair sample of the Universe [7]. There is very little power at the fundamental mode, even at $z = 0$: $\Delta^2(k_f, z = 0) < 10^{-4}$. The lowest few modes obey linear growth to sub-percent accuracy and we run enough different realizations to ensure that the spectrum at the scales of interest is well determined. The large number of particles ensures that the spectrum is well converged for the k -modes of interest, which we checked explicitly by comparing simulations of different box sizes. The simulations are evolved from $z_i = 100$, with the particles perturbed from an initially uniform grid using the Zel’dovich approximation. The rms particle move was about 5% of the mean interparticle spacing. Comparison with second order Lagrangian perturbation theory initial conditions showed that this starting redshift is sufficiently high that transients from the Zel’dovich start are irrelevant for the scales and redshifts of interest.

Most of the evolutions were performed with a parallel particle-mesh code. To cross-check our results we used two high force resolution N-body codes: the TreePM code [36] and Gadget-II [37]. These have each been tested against a suite of other codes [7, 8, 9], with very good agreement. We ran a subset of our simulations using all three codes to quantify the level of precision for the box size and particle loading of relevance here. With its default time stepping, the TreePM code produces dark matter power spectra in agreement with those from Gadget-II to better than 0.2% out to $k \simeq 1 h \text{ Mpc}^{-1}$ and to $\mathcal{O}(10^{-4})$ for $k < 0.1 h \text{ Mpc}^{-1}$. However these runs prove to be quite time consuming. If we set the time step in the

TreePM code to

$$(\delta \ln a)^{-2} = \left[\frac{1}{0.05} \right]^2 + \left[\frac{a}{0.01} \right]^2, \quad (8)$$

which evolves from 5% steps at early times to 1% steps as $a \rightarrow 1$, we find a shortfall of power of approximately 1% at $k \simeq 1 h \text{Mpc}^{-1}$ but very little difference for $k < 0.1 h \text{Mpc}^{-1}$. We choose the same time stepping for the particle-mesh code, which results in very short run times allowing an ensemble of simulations to be performed. With this step the particle-mesh power spectra show a significant deficit of power (compared to TreePM or Gadget-II) beyond $k \approx 0.7 h \text{Mpc}^{-1}$ but for $k < 0.2 h \text{Mpc}^{-1}$, the region of interest here, the agreement is better than 1%.

To compute the power spectrum at different output times the particles were binned onto a regular, Cartesian grid using charge-in-cell assignment [38] and the resulting density field was Fourier transformed. The Fourier modes were squared, corrected for the gridding by dividing by the Fourier transform of the charge assignment scheme, and binned into bins equally spaced in $\log k$. The average of $\Delta^2(k)$ was assigned to the average k in the bin and shot-noise was subtracted assuming it was Poisson. The binning introduces artifacts at low k , where the sampling on the grid is sparse and the dimensionless power spectrum is steep, but these are small for the scales of most relevance to us. Similarly there is some evidence that the shot-noise in simulations is not scale-invariant (Poisson), but the correction is negligibly small on the scales of interest here.

The non-linear propagator was computed by cross-correlating the initial density field with the final one [14]. Similar to the power spectrum, this quantity is obtained by Fourier transforming both fields, multiplying their Fourier coefficients, correcting for gridding, and then binning the results.

The velocity statistics are more problematic, because while the density and momentum fields must vanish where there are no tracer particles, the same is not true of the velocities. Thus estimates of the velocity field must employ a smoothing technique. Similarly the velocity field is more sensitive to finite force resolution. On the other hand comparison of the velocity fields with the density fields is less sensitive to finite volume scatter. For this reason we use a different set of simulations, with more particles (up to 3 billion) in smaller boxes ($1.25 h^{-1} \text{Gpc}$ down to $720 h^{-1} \text{Mpc}$) evolved with the TreePM code, for the velocity statistics. Comparison with different smoothing schemes, box sizes and particle loadings show that with these choices our results are well converged on the scales of interest [39].

IV. COMPARISON

A. The Power Spectrum

We begin our analysis by comparing the predictions of SPT against our simulation results. Figure 1 shows the linear theory, 1-loop SPT, and 2-loop SPT power spectrum for ΛCDM and $c\text{CDM}$. While 2-loop SPT is a marked improvement over 1-loop SPT at $z = 1$, it's actually worse than 1-loop at $z = 0$. The effect is most apparent in $c\text{CDM}$, which has larger σ_8 and Ω_b . This break-down in standard perturbation theory is not entirely surprising: since the n^{th} order term in SPT goes like $D^{2n}(z)$, at any given scale one expects higher order terms to become comparable in magnitude to lower order terms at sufficiently late times. Our results suggest that at BAO scales (roughly $k = 0.05 - 0.25 h \text{Mpc}^{-1}$) the break-down occurs between $z = 1$ and $z = 0$.

A common heuristic prescription dictates that 1-loop SPT can be trusted to 1% for wavenumbers satisfying $\Delta_L^2(k) \lesssim 0.4$ [41]. On the other hand a strict application of perturbation theory implies that 1-loop SPT can be trusted to 1% for wavenumbers where the 2-loop contribution is 1% of linear theory. In Figure 1 we indicate the predicted domain of validity of 1-loop SPT according to these two criteria. For comparison we also indicate where the 2-loop contribution is within 3% of linear theory. One sees that the agreement with simulations is slightly better than what our more rigorous criterion suggests. For instance for ΛCDM at $z = 0$, $\Delta_L^2 = 0.4$ at $k_* \approx 0.12 h \text{Mpc}^{-1}$. At this wavenumber 1-loop SPT overshoots the reference spectrum by about 3%, whereas 2-loop SPT undershoots the reference spectrum by 5%. For $c\text{CDM}$ at $z = 0$ the situation is much worse, with 1-loop SPT overshooting by only 6% at $k_* \approx 0.11 h \text{Mpc}^{-1}$, but 2-loop SPT undershooting by almost 20%.

RPT and closure theory have also been developed to two loops. Given the above conclusions about SPT, it is natural to make the same comparison between the 1-loop and 2-loop predictions from RPT and closure theory. In Figure 2 we show the matter power spectrum for these theories at tree, 1-loop, and 2-loop order for both ΛCDM and $c\text{CDM}$. For closure theory it appears that going to 2-loop order extends the range of agreement with simulations, although the wiggles of the power spectrum are not matched in detail. For RPT, as with SPT, the 2-loop result is systematically high, whereas the 1-loop result performs fairly well below $k \approx 0.15 h \text{Mpc}^{-1}$. Agreement with simulations can be improved by changing the damping scale in the propagator. In [22] the damping scale was modified by calculating Σ with the linear theory expression (Eq. 7), but using the non-linear power spectrum and integrating only up to $k = 4 k_{\text{nl}}$. This leads to a $\sim 10\%$ additional suppression of $G(k)$ and hence $P(k)$ on the relevant scales, bringing the theory into better agreement with simulations [22]. At present this correction has not been derived from first principles and we have not included it, but it appears that improvements

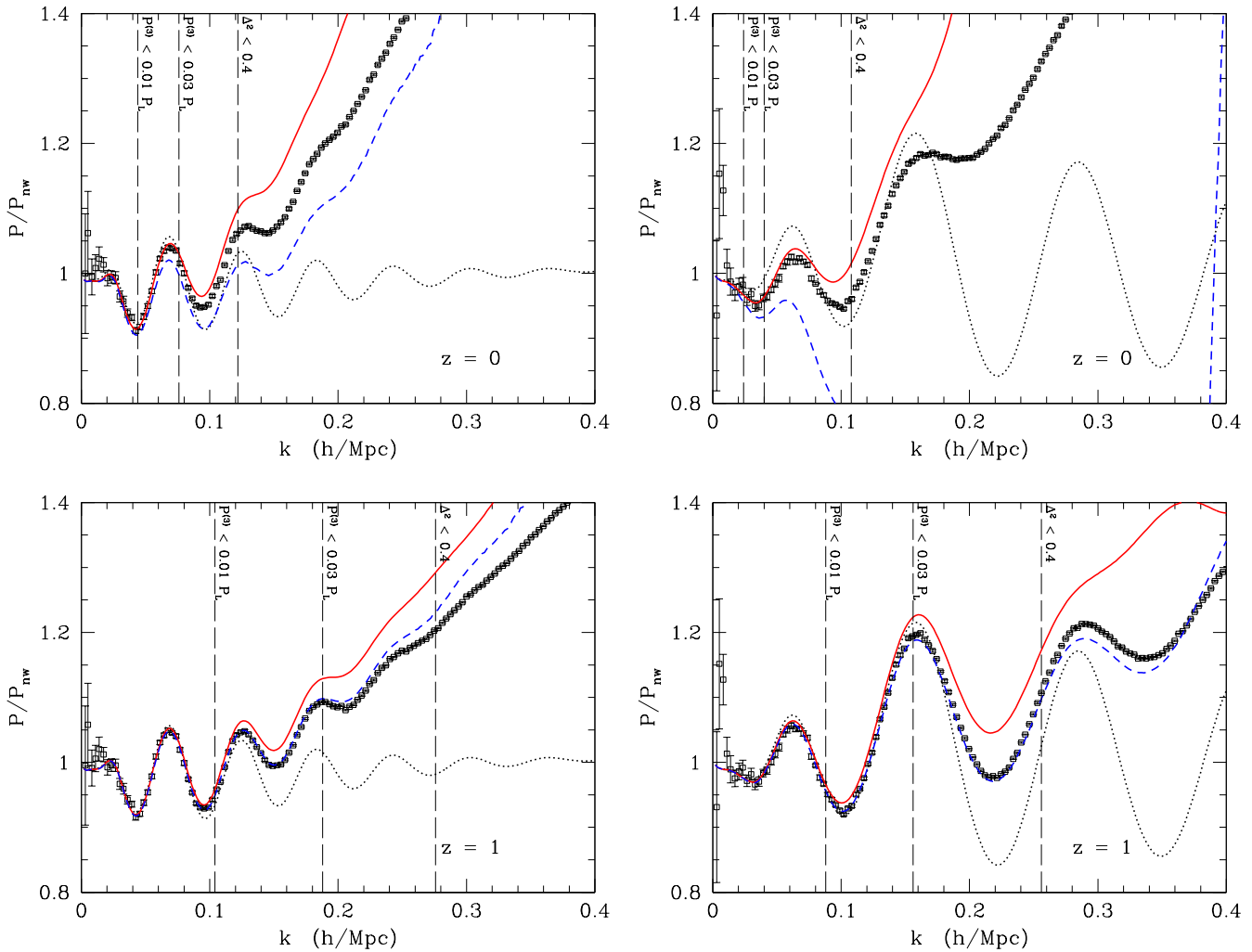


FIG. 1: SPT power spectrum at linear (black; dotted), 1-loop (red; solid), and 2-loop (blue; dashed) order. The squares with error bars show the mean and error from our N-body simulations. The four panels show Λ CDM (left) and c CDM (right) at redshifts 1 (top) and 0 (bottom). Each curve has been divided by the no-wiggle power spectrum of [40] to reduce the dynamic range. We also indicate the domain of validity of 1-loop SPT according to the heuristic prescription of [41] ($\Delta^2 < 0.4$), and according to the criterion $P^{(3)} < \alpha P_L$ for $\alpha = 0.01, 0.03$.

in this direction could be important.

Figure 3 shows the predicted power spectrum for the remainder of the theories that we consider in this work. With Figures 1 and 2, these figures give an overview of the agreement between our N-body simulations and the perturbation theories for Λ CDM and c CDM. Some of the trends can be seen easily in these figures, and are generic across cosmologies and redshifts. For instance 1-loop SPT, which is the same as 1-loop LPT, always over-predicts $P(k)$ at high k . Lagrangian resummation theory on the other hand is much too strongly damped beyond the first wiggle. Large- N theory more or less traces 1-loop SPT before turning over, while time-RG theory and RGPT follow the general trends of the N-body data without fitting any particular feature precisely. (Note that the nearly perfect agreement between RGPT and sim-

ulations for c CDM at $z = 1$ is likely spurious, as this level of agreement is not seen for other cosmologies or at other redshifts.) RPT and closure give nearly identical tree-level predictions, and very similar 1-loop predictions for $P(k)$. Closure theory appears to benefit greatly from going to 2-loop order, whereas for RPT even at $z = 1$ it appears that 2-loop does worse than 1-loop.

While we have run many realizations of each cosmology to reduce run-to-run variance, one sees in Figures 1, 2 and 3 that the N-body data are still noisy at low k , which makes it difficult to make quantitative statements about the performance of the perturbation theories. To overcome this we define a ‘reference spectrum’ which interpolates the N-body results at high and intermediate k with the 1-loop SPT calculation at low k . This eliminates the large scatter from the finite number of modes

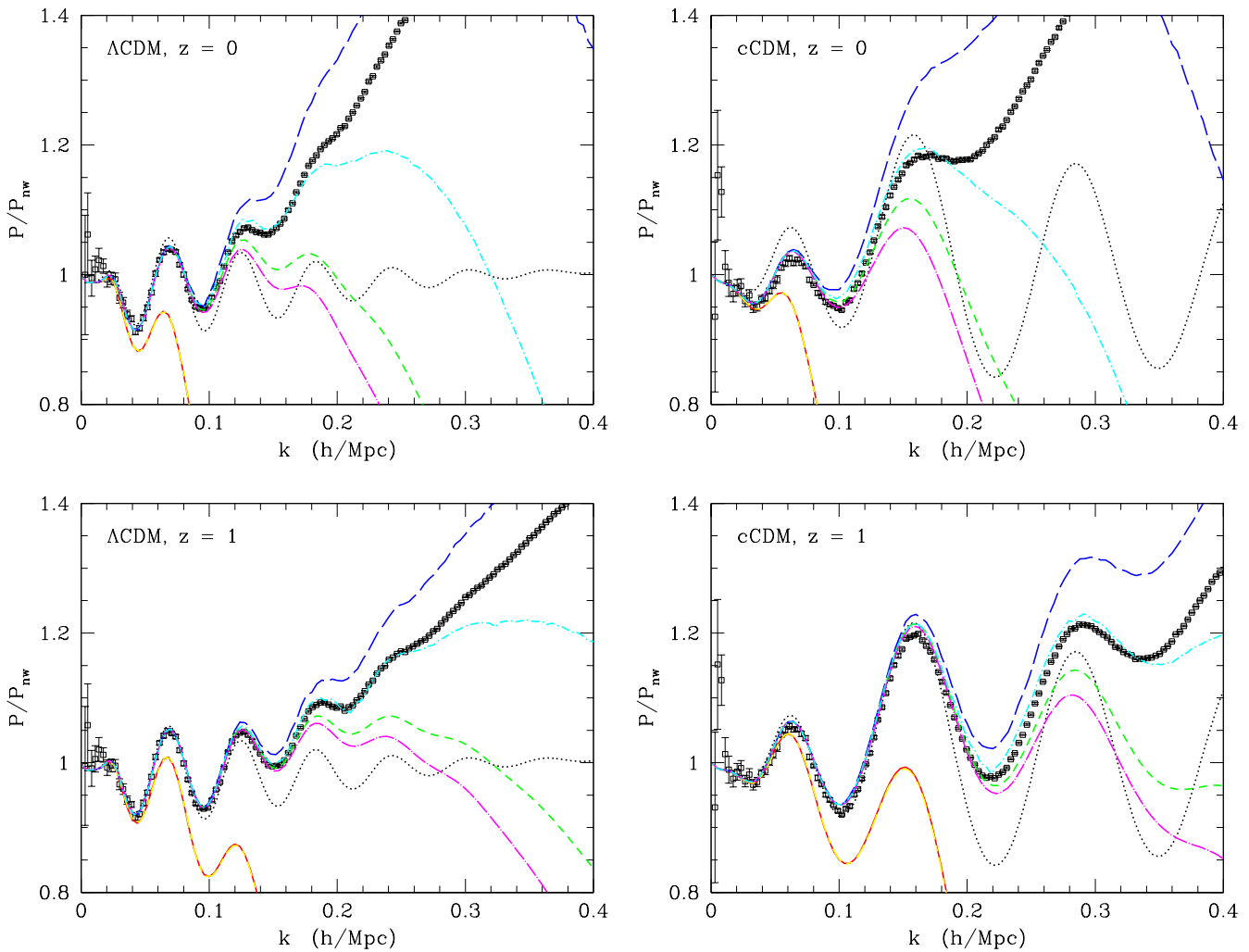


FIG. 2: Comparison of the tree-level, 1-loop and 2-loop power spectrum from RPT and closure theory, for Λ CDM (left) and c CDM (right). Each curve has been divided by the no-wiggle power spectrum of [40] to reduce the dynamic range. The (black) dotted line is linear theory, the (red) solid line is tree-level RPT, the (green) dashed line is 1-loop RPT, the (blue) long-dashed line is 2-loop RPT, the thick (yellow) short-long dashed line is tree-level closure, the (magenta) dot-long dashed line is 1-loop closure, and the (cyan) dot-dashed line is 2-loop closure.

in the simulations and any biases from the finite bin sizes at low k , while still retaining the information from the simulations at larger k . This gives a smooth function, defined for all k , which can be used as a reference to make a quantitative comparison. Given the large number of simulations we have run, the uncertainty in the N-body results is small before perturbation theory becomes invalid and we can see a significant range of k for which theory and simulation agree well. This makes our final results insensitive to how the matching is done. Our recipe for producing a reference spectrum is to treat both the N-body results and 1-loop SPT as independent measurements of the true power spectrum, with errors given by the run-to-run variance within a wavenumber bin [54] in the former case, and by the 2-loop SPT term in the latter case. Then the reference spectrum at any given k is

defined by fitting a polynomial to all available measurements within a small wavenumber range $[k - \Delta k, k + \Delta k]$ and evaluating that polynomial at k . For simplicity we chose to fit to a cubic with $\Delta k = 0.01 h \text{Mpc}^{-1}$, though the resulting reference spectrum is rather insensitive to these choices.

All of the theories beyond linear correctly predict the ‘dip’ below linear theory which can be most clearly seen in Figure 4 around $k \simeq 0.04 h \text{Mpc}^{-1}$. This is sometimes referred to as pre-*virialization*, and arises because the non-linear growth of the density and velocity fields is slower than linear on scales where the effective spectral index is more positive than (about) -1.5 (see [12] for further discussion). In this region use of any of the methods provide significant improvements over linear theory.

To gain an overview of the range of validity of the

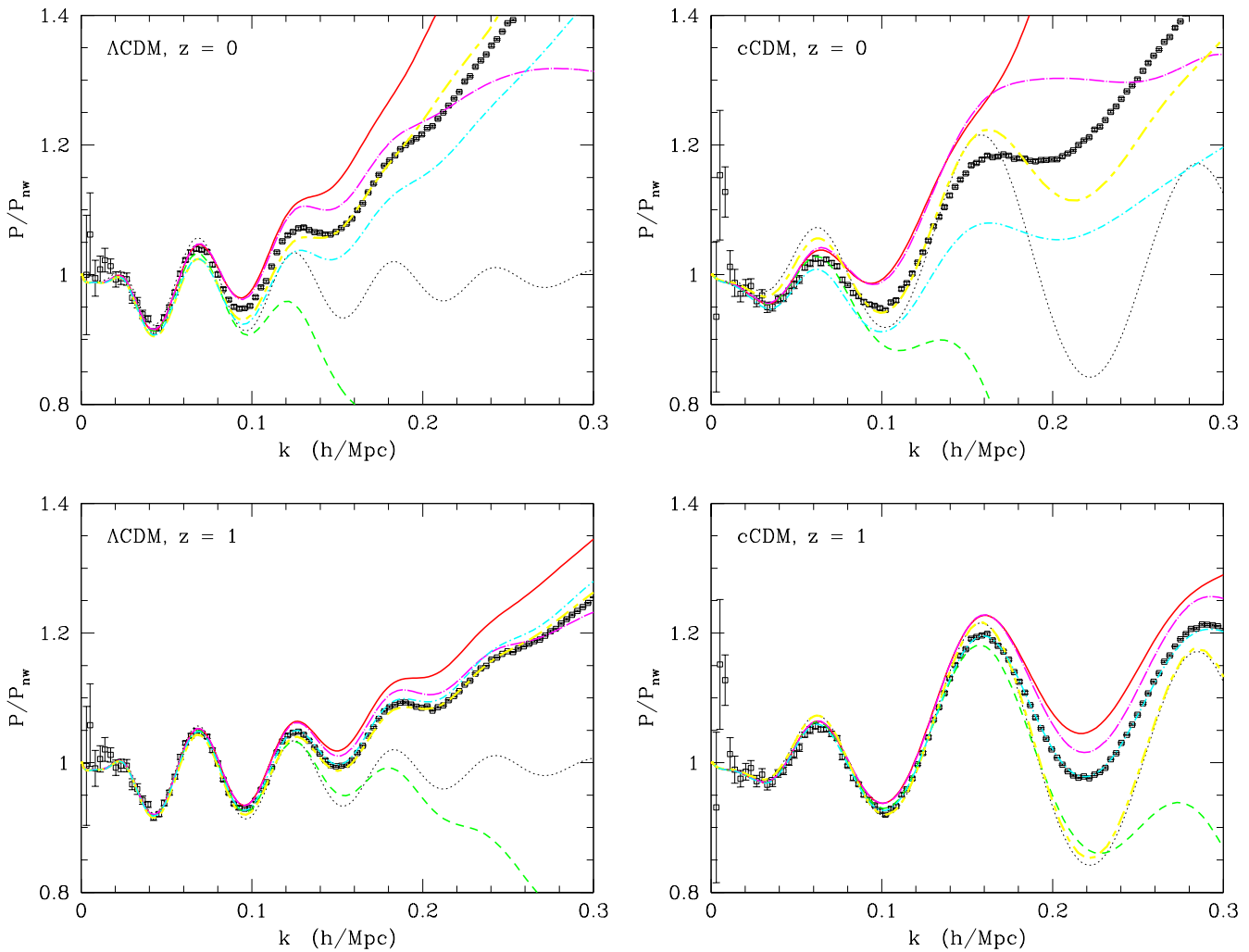


FIG. 3: Comparison of the power spectrum for the remaining theories. Each curve has been divided by the no-wiggle power spectrum of [40] to reduce the dynamic range. The (red) solid line is 1-loop SPT, the (magenta) dot-long dashed line is large- N theory, the (green) dashed line is Lagrangian resummation, the thick (yellow) short-long dashed line is time-RG theory, and the (cyan) dot-dashed line is RGPT.

Methods	$k_{\max}(z)$				
	$z = 0$	0.3	0.7	1	1.5
Linear	0.03	0.08	0.09	0.09	0.09
1-loop SPT [16, 17, 18, 19, 20, 21]	0.08	0.10	0.11	0.13	0.14
2-loop SPT [42]	0.04	0.06	0.09	0.23	0.20
1-loop RPT [13, 14, 22]	0.10	0.13	0.15	0.16	0.20
2-loop RPT	0.08	0.08	0.11	0.11	0.13
1-loop Closure [2]	0.09	0.10	0.14	0.15	0.18
2-loop Closure	0.08	0.13	0.17	0.27	0.21
Time-RG [24]	0.04	0.05	0.06	0.09	0.10
Large-N [30]	0.08	0.11	0.12	0.14	0.17
Lag.Resum [31]	0.07	0.08	0.09	0.10	0.13

TABLE II: The methods we consider in this work and the lowest k (in $h\text{Mpc}^{-1}$) at which each method departs from our reference spectrum by 1%, as a function of redshift for our chosen ΛCDM cosmology.

various methods we list in Table II the smallest value of k at which each method departs from our reference spectrum by 1% for ΛCDM (a comparison with other schemes defined in the literature is presented in Table III). As expected, the methods perform better at smaller scales the higher the redshift. All of the methods outperform linear theory, owing to the marked effects of previrialization, however none of the methods appear to be accurate beyond $k \simeq 0.1 h\text{Mpc}^{-1}$ at $z = 0$.

B. Testing the dynamics

While comparison of the power spectrum is the most common test for perturbation theory, it is also useful to test if perturbation theory is correctly describing the underlying dynamics. To do so, we examine some of the

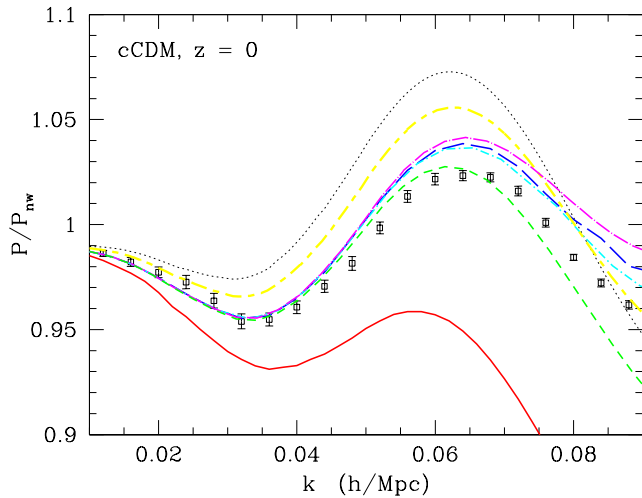


FIG. 4: Comparison between analytic models for $P(k; z = 0)$ and the reference spectrum (Section IV) for model $c\text{CDM}$, focusing on large scales. Each curve has been divided by the no-wiggle power spectrum of [40] to reduce the dynamic range. The points with error bars are the ‘reference spectrum’ defined in the text. The (black) dotted line is linear theory, the (red) solid line is 2-loop SPT, the (blue) long-dashed line is 2-loop RPT, the (green) short-dashed line is Lagrangian resummation, the (cyan) dot-dashed line is 2-loop closure theory, the thick (magenta) dot-long dashed line is the large- N expansion, and the thick (yellow) short-long dashed line is time-RG theory.

Ref.	Method	ΛCDM		$c\text{CDM}$	
		$z = 0$	$z = 1$	$z = 0$	$z = 1$
[41]	SPT	0.12	0.28	0.07	0.25
[43]	SPT	0.10	0.19	0.08	0.19
[3]	SPT	0.08	0.09	0.08	0.09
[31]	Lag.R.	0.08	0.13	0.07	0.15
[3]	RPT	0.09	0.09	0.09	0.10
[3]	Closure	0.09	0.09	0.09	0.10

TABLE III: The value of k , in $h\text{Mpc}^{-1}$, to which various flavors of perturbation theory can be trusted according to various published criteria. See [3] for discussion.

constituent pieces from the simulations, and compare to the perturbation theory predictions.

Figure 6 compares the non-linear propagator

$$\tilde{G}_1(k) = G_{11}(k) + G_{12}(k) \sim \frac{\langle \delta_{\text{NL}} \delta_L^* \rangle}{\langle \delta_L \delta_L^* \rangle} \quad (9)$$

from the simulations with the predictions of analytic models. Only RPT and Lagrangian resummation give the expected behavior, $\tilde{G}_1 \rightarrow 0$, for large k .

Comparisons of perturbation theory with simulations typically focus on the density auto-correlation function or power spectrum. However perturbation theory also makes predictions for the (irrotational) velocity field which can be checked against simulations. In Figure 7

we show the cross-correlation coefficient

$$r(k) \equiv P_{\delta\theta}(k) / \sqrt{P_{\delta\delta}(k)P_{\theta\theta}(k)} \quad (10)$$

for several theories, compared with the same quantity measured from simulations. In linear theory $r(k) = 1$ identically. On physical grounds one expects to see a decoherence of density and velocity fields on small scales, and indeed the simulations show $r(k) \rightarrow 0$ for large k . None of the analytic theories correctly reproduce this behavior. SPT and Time-RG theory follow the downward turn of the simulation data initially, but then predict an unphysical $r(k) > 1$ very soon after non-linear corrections become important. RPT and closure theory perform somewhat better, in that $r(k)$ never exceeds unity, but the level of agreement with simulations is still not good above $k \simeq 0.1 h\text{Mpc}^{-1}$. (Note that we have displayed here only the 1-loop predictions from these theories.) The deviation in $r(k)$ seems to be driven mostly by the densities, with perturbation theory performing better at the same scale for the velocities than the densities (see Figure 8).

V. DISCUSSION

Standard perturbation theory has a simple and direct theoretical motivation, and results in explicit integral expressions at any order. If taken to infinite order, it provides an exact solution (though to an idealized problem). While standard perturbation theory works well at high redshift and large scales, our results indicate that the standard expansion is badly behaved at the redshifts and scales most accessible to observation, in that higher order terms are comparable in magnitude to lower order terms. Although one expects the expansion to converge if taken to sufficiently high order, this comes at a great computational cost. With advances in raw computing power it may one day become possible to perform the calculation to the requisite order, but in the near future this approach seems impracticable.

On the other hand, it should be emphasized that SPT performs rather well at high redshifts, $z \gtrsim 1$. Figure 1 shows that 2-loop SPT at $z = 1$ agrees with simulations to 1% out to $k = 0.2 h\text{Mpc}^{-1}$ or beyond (where the simulations themselves become unreliable). At these redshifts SPT not only provides a reasonable theoretical prediction for the matter power spectrum on observationally relevant scales, but also an estimate of the theoretical uncertainty on this prediction.

RPT is essentially a rearrangement of the standard expansion, so like SPT it is an exact solution if carried out to all orders. While this rearrangement appears to improve the convergence properties of the perturbation series, it makes it unclear what small quantity (if any) we are actually expanding in. Furthermore, RPT does not actually provide closed-form expressions for the power spectrum, but rather integral relations where P_{ab}

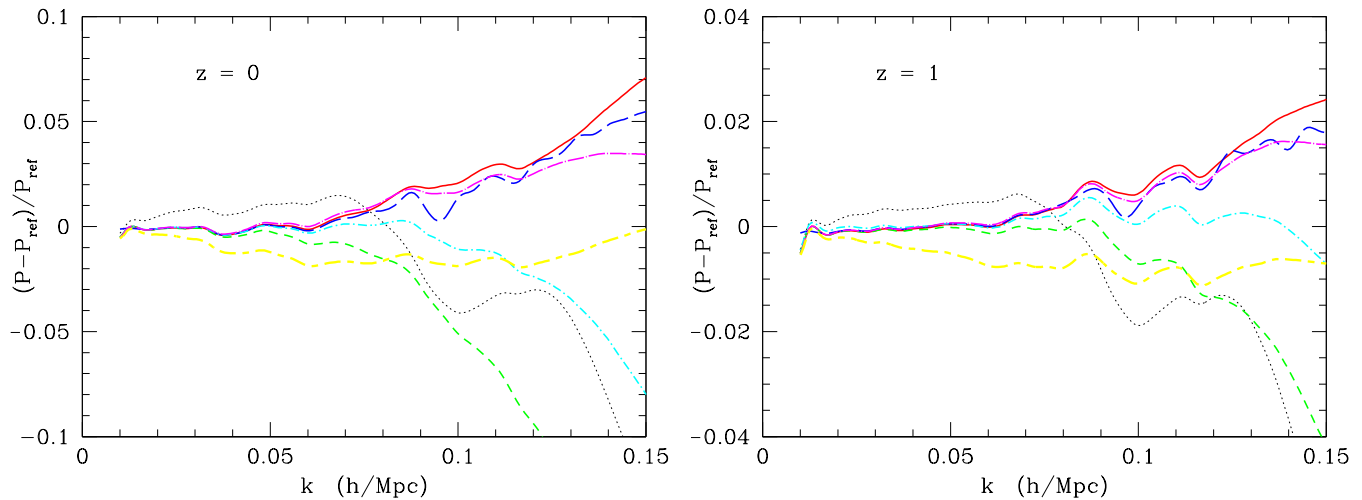


FIG. 5: The fractional deviation of each method from the reference spectrum, for Λ CDM at $z = 0$ (left) and $z = 1$ (right). This figure focuses on the region $k < 0.15 h \text{ Mpc}^{-1}$ where linear theory is inadequate but higher order methods are still viable. As in Figure 4 the (black) dotted line is linear theory, the (red) solid line is 2-loop SPT, the (blue) long-dashed line is 2-loop RPT, the (green) short-dashed line is Lagrangian resummation, the thick (cyan) dot-short dashed line is 2-loop closure theory the thick (magenta) dot-long dashed line is the large- N expansion, and the thick (yellow) short-long dashed line is time-RG theory.

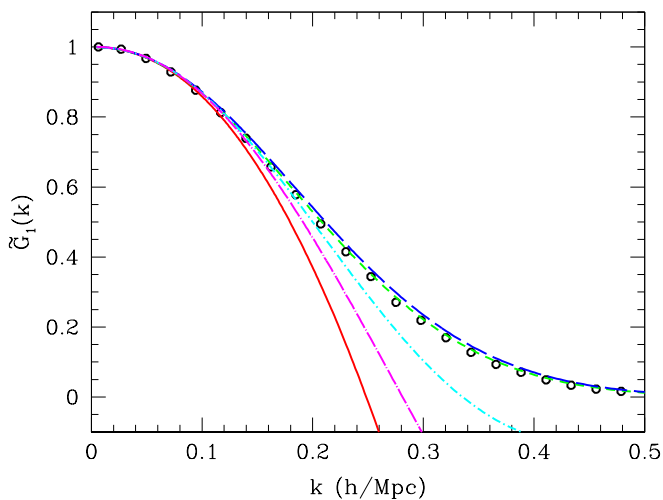


FIG. 6: The non-linear propagator (normalized to 1 at $k = 0$) for Λ CDM at $z = 0$. The (red) solid line is SPT, the (green) short-dashed line is Lagrangian resummation, the (blue) long-dashed line is RPT, the thick (cyan) dot-short dashed line is closure theory and the thick (magenta) dot-long dashed line is the large- N expansion.

is expressed in terms of mode-coupling integrals of itself. Thus in addition to truncating the loop expansion at finite order, a fully consistent implementation of RPT requires solving for P_{ab} according to an iterative scheme, of which the explicit expressions presented in [22] represent only the first step. The error associated with this approximation has (to our knowledge) yet to be quanti-

fied.

Closure theory derives from a very different perturbative scheme than RPT, yet the results obtained are superficially quite similar. There is no obvious way to provide error estimates on the results of closure theory, however, as the closure equations are obtained from heuristic approximations rather than a systematic expansion. Furthermore the propagator in closure theory shows unrealistic oscillations for large k . As mentioned previously, the closure equations are solved approximately in [2] by means of a Born-like expansion. Recently [44] an attempt has been made to solve the closure equations numerically without resort to such a Born-like expansion. The resulting predictions for the power spectrum appear to agree better with simulations than the results presented here, although it is difficult to draw any firm conclusions from the information provided.

Time-RG theory is based on a single well-defined approximation: the vanishing of the trispectrum. The validity of this approximation can easily be checked in simulations, and in principle this could allow one to quantify the theoretical uncertainty in the method. As most easily seen in Figure 5, although time-RG theory follows the general trends of our reference spectrum over a wider range than other methods, it comes up short by 1-2% over the entire quasi-linear regime. It also gives an unphysical prediction for the density-velocity cross-correlation.

The large- N expansion utilizes more sophisticated theoretical machinery than other resummation techniques. While the path-integral formalism for computing clustering statistics is exact, the errors introduced by the large- N expansion are difficult to quantify, as ‘ N ’ is a fictitious

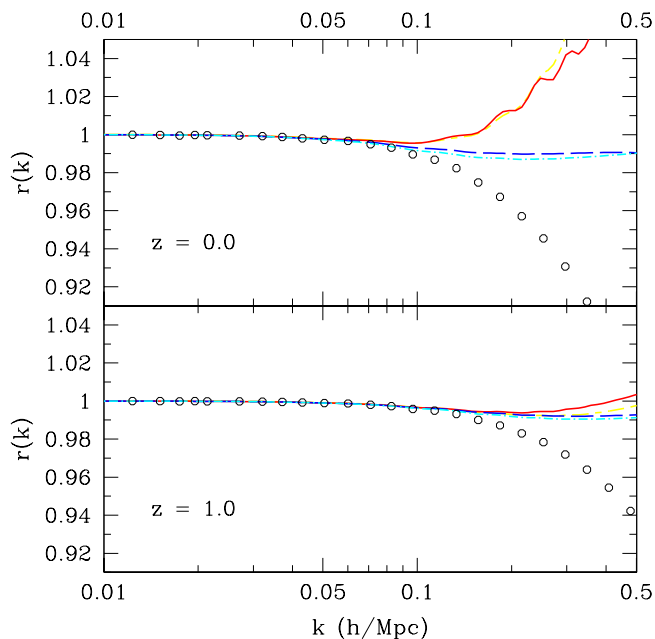


FIG. 7: A comparison of the density-velocity cross-correlation predicted analytically with that measured in simulations, for Λ CDM at redshift $z = 0$ (top) and $z \approx 1$ (bottom). As in Figure 4, the solid (red) line is SPT, the dashed (blue) line is RPT, the dot-dashed (cyan) line is closure theory, and the short-long-dashed (yellow) line is Time-RG theory. For simplicity we show only the 1-loop predictions for SPT, RPT, and closure theory.

parameter. Although the large- N expansion corresponds to an infinite partial resummation of the standard perturbative expansion, from our results it seems that this resummation offers little improvement over 1-loop SPT in the quasi-linear regime. The grossly unphysical behavior of the propagator in this theory is likely responsible for this effect. As mentioned previously, we have focused attention on the steepest-descent method rather than the 2PI effective action method of [30]. The latter method produces a more reasonable propagator, and likely results in a better prediction for the power spectrum, although at an increased computational cost.

Like SPT, the Lagrangian resummation prescription of [31] also results in easy to compute, explicit integral expressions. These are well behaved at large k , allowing e.g. $\xi(r)$ to be computed, and there are natural extensions to redshift space and to halo bias [32]. For the real-space mass power spectrum considered here it offers a marginal improvement over 1-loop SPT for $k\Sigma < 1/2$, although the damping prefactor strongly overcompensates as one moves further into the quasi-linear regime.

Our results have interesting implications for generating a suite of simulations aimed at constraining the matter power spectrum. If we can trust perturbative methods for $k\Sigma < x_c$, then we can focus the computational resources on higher k . Assuming Gaussian fluctuations, obtaining 1% accuracy in a bin $(k; \Delta k)$ requires 2×10^4

k	$\Delta_{\text{lin}}^2(k)$	$\Delta_{\text{ref}}^2(k)$	$G(k)$
0.02	0.012	0.012	0.996
0.04	0.053	0.053	0.980
0.06	0.130	0.129	0.950
0.08	0.210	0.210	0.914
0.10	0.274	0.285	0.859
0.12	0.398	0.410	0.804
0.14	0.466	0.507	0.737
0.16	0.533	0.617	0.664
0.18	0.662	0.764	0.592
0.20	0.720	0.894	0.518

TABLE IV: Our input linear theory spectrum, at $z = 0$, for the Λ CDM model as a function of wavenumber (in $h \text{ Mpc}^{-1}$) and the reference spectrum and propagator $[G(k)]$ from our N -body simulations. Our convergence tests indicate the spectra should be accurate to $< 1\%$ over the range of scales shown.

modes. There are $(kL_{\text{box}})^3 (\Delta k/k)/(2\pi^2)$ modes from a periodic box of side length L_{box} , so our 1% constraint at $k\Sigma \simeq x_c$ translates into

$$L_{\text{box}} \simeq \frac{\Sigma}{x_c} \left(\frac{2\pi^2 N}{\Delta k/k} \right)^{1/3} \approx 3 \text{Gpc} \left(\frac{0.5}{x_c} \right) \left(\frac{\Sigma}{10 \text{Mpc}} \right) \left(\frac{N}{2 \times 10^4} \right)^{1/3} \left(\frac{0.1}{\Delta k/k} \right)^{1/3} \quad (11)$$

or an equivalent volume of smaller simulations. This constraint is most difficult to meet at $z = 0$, since Σ is larger and the simulations must be evolved for longer. As an example with the default parameters listed above we would require 27 simulations, each $1 h^{-1} \text{Gpc}$ on a side, to obtain percent level constraints on the power spectrum of Λ CDM in a 10% band near $k \simeq 0.1 h \text{ Mpc}^{-1}$ at $z = 0$ but at $z = 1$ we could trust perturbation theory at this scale and focus the simulations on $k \simeq 0.15 h \text{ Mpc}^{-1}$ where three times fewer simulations of the same size are needed.

VI. CONCLUSIONS

Perturbative methods have a long history in cosmology, and are widely used in many fields of physics. Many of the techniques reviewed herein were first developed in other fields and applied to other problems, with varying levels of success, before being pressed into service for modeling cosmological perturbations. In this paper we have studied a variety of these methods as applied to predicting the large-scale clustering of cold, collisionless matter in an expanding Universe. Our results indicate that the analytic theories correctly model the approach to non-linearity and work well when the perturbations are small, but none of the available theories are up to the challenge of fully describing the behaviour of matter on quasi-linear scales at late times. We have emphasized the need to study a range of different cosmologies and to look at a variety of different statistical observables, as accidental agreement between theory and simulations is

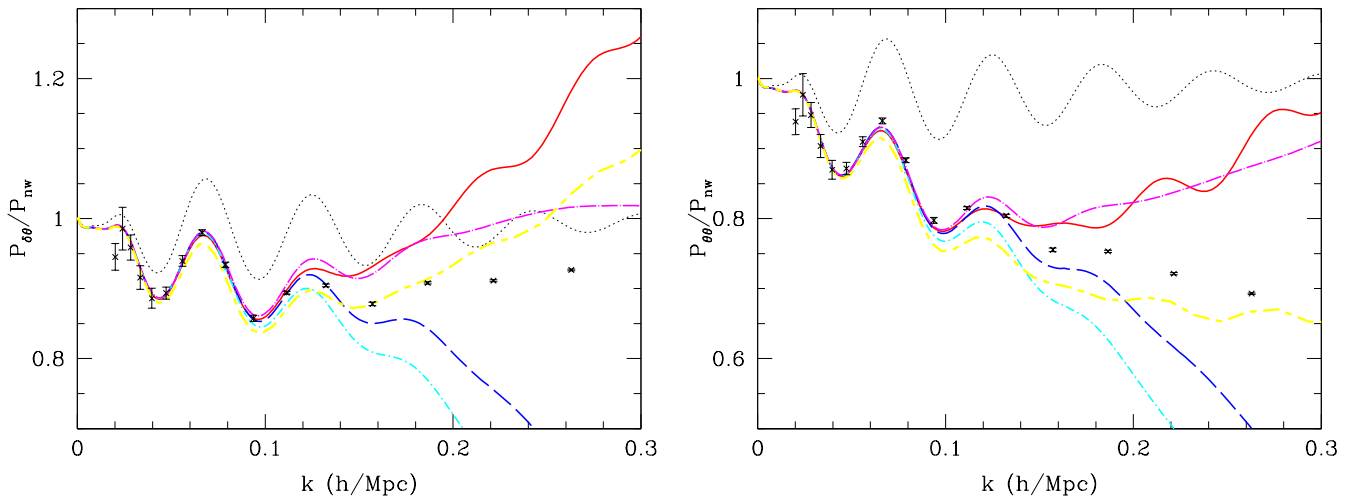


FIG. 8: The density-velocity cross spectrum (left) and the velocity-velocity auto-spectrum (right) for the Λ CDM model at $z = 0$. As in Figure 7 the (black) dotted line is linear theory, the (red) solid line is 1-loop SPT, the (blue) long-dashed line is 1-loop RPT, the (cyan) dot-short dashed line is 1-loop closure theory, the thick (magenta) dot-long dashed line is large- N theory, and the thick (yellow) short-long dashed line is time-RG theory.

possible if one only considers the power spectrum. We have computed the 2-loop contribution to SPT and found that the standard perturbative expansion is badly behaved at low redshifts, even on scales where 1-loop SPT was previously believed to be valid. This provides further motivation for studying alternative analytic approaches based on non-perturbative methods, though at the same time it emphasizes the need for error control in analytic methods.

This work has made use of a large number of high dynamic range N-body simulations, against which we can compare the analytic models. We make these data public in Table IV to aid future work in the field. In addition a flexible software package that implements the perturbation schemes described in this paper is available from the authors.

Acknowledgments

We thank Román Scoccimarro, Martín Crocce, Pat McDonald, Salman Habib, and Katrin Heitmann for helpful discussions. The simulations presented in this paper were carried out using computing resources of the National Energy Research Scientific Computing Center and the Laboratory Research Computing project at Lawrence Berkeley National Laboratory. NP is supported by NASA Hubble Fellowship NASA HST-HF-01200.01 and an LBNL Chamberlain Fellowship.

APPENDIX A: EULERIAN PERTURBATION THEORY

Here we briefly recap the derivation of the fluid equations in the Eulerian picture, and the assumptions that are made in perturbative treatments ([16, 17, 18, 19, 20, 21]; see [12] for a review). The matter content of the Universe is modeled as a large collection of identical particles of mass m , interacting only through mutual gravitational attraction. For low densities and sub-horizon scales, such forces are adequately described by Newtonian gravity in a uniformly expanding background, with the Newtonian potential sourced by inhomogeneities in the density field. The distribution function for such a set of particles obeys the Vlasov equation. The N-body methods are essentially a Monte-Carlo evolution of the Vlasov equation where the Monte-Carlo tracer super-particles move along characteristics.

Analytically one typically invokes the *single-stream approximation*, which assumes that all particles at a given point \mathbf{x} move together with the same velocity $\mathbf{v}(\mathbf{x})$. This amounts to demanding that $f(\mathbf{x}, \mathbf{p}) \propto \delta_D[\mathbf{p} - m\mathbf{v}(\mathbf{x})]$, where f is the distribution function and δ_D is the Dirac delta function. This assumption is explicitly violated once shell crossing occurs in gravitational collapse, but is thought to be a reasonable approximation for small density contrasts. The

velocity moments of the Vlasov equation then give the familiar fluid equations (e.g. [19])

$$\frac{\partial \delta}{\partial \tau} + \nabla \cdot [(1 + \delta)\mathbf{v}] = 0, \quad (\text{A1})$$

$$\frac{\partial \mathbf{v}}{\partial \tau} + \mathcal{H}\mathbf{v} + (\mathbf{v} \cdot \nabla)\mathbf{v} + \nabla\Phi = 0. \quad (\text{A2})$$

where $\mathcal{H} = d \ln a / d\tau = aH$ is the conformal Hubble parameter.

It is conventional to further assume that the vorticity $\mathbf{w} = \nabla \times \mathbf{v}$ of the velocity field vanishes, i.e. that the fluid is *irrotational*. This assumption is motivated by noting that $\mathbf{w} \propto a^{-1}$ at linear order, and is well supported by simulations [45, 46]. Under this approximation the velocity field is completely specified by its divergence $\theta = \nabla \cdot \mathbf{v}$, and the fluid equations reduce to

$$\frac{\partial \delta}{\partial \tau} + \theta = -\nabla \cdot (\delta \mathbf{v}), \quad (\text{A3})$$

$$\frac{\partial \theta}{\partial \tau} + \mathcal{H}\theta + 4\pi G a^2 \bar{\rho} \delta = -\nabla \cdot [(\mathbf{v} \cdot \nabla)\mathbf{v}]. \quad (\text{A4})$$

In Fourier space $\mathbf{v}(\mathbf{k}) = -i\mathbf{k}\theta(\mathbf{k})/k^2$, giving

$$\frac{\partial \delta(\mathbf{k})}{\partial \tau} + \theta(\mathbf{k}) = - \int \frac{d^3 q_1 d^3 q_2}{(2\pi)^3} \delta_D(\mathbf{q}_1 + \mathbf{q}_2 - \mathbf{k}) \frac{\mathbf{k} \cdot \mathbf{q}_1}{q_1^2} \theta(\mathbf{q}_1) \delta(\mathbf{q}_2), \quad (\text{A5})$$

$$\frac{\partial \theta(\mathbf{k})}{\partial \tau} + \mathcal{H}\theta(\mathbf{k}) + \frac{3}{2}\Omega_m \mathcal{H}^2 \delta(\mathbf{k}) = - \int \frac{d^3 q_1 d^3 q_2}{(2\pi)^3} \delta_D(\mathbf{q}_1 + \mathbf{q}_2 - \mathbf{k}) \frac{k^2 (\mathbf{q}_1 \cdot \mathbf{q}_2)}{2q_1^2 q_2^2} \theta(\mathbf{q}_1) \theta(\mathbf{q}_2). \quad (\text{A6})$$

As long as δ and θ are small, the right-hand sides of the fluid equations are small and can be dropped; this approximation defines linear theory. The solution to the resulting linearized fluid equations may be written as

$$\delta_L(\mathbf{k}; z) = \frac{D(z)}{D(z_i)} \delta_i(\mathbf{k}) \quad , \quad \theta_L(\mathbf{k}; z) = -\mathcal{H}(z)f(z) \frac{D(z)}{D(z_i)} \delta_i(\mathbf{k}), \quad (\text{A7})$$

where δ_i is the density contrast at some early time z_i when linear theory is certainly valid, D is the linear growth function (normalized to 1 today), and $f \equiv d \ln D / d \ln a$. At early times $\Omega_m \approx 1$ and $D \propto a$. Note that a possible decaying mode contribution, proportional to $a^{-3/2}$ at early times, is forced to zero in linear theory by the condition that δ be well-behaved as $a \rightarrow 0$. Note also that the mode-coupling integrals vanish for $\mathbf{k} = 0$, so linear theory is always valid in some neighborhood of $\mathbf{k} = 0$, even at late times. For convenience we define δ_0 to be the linear density contrast today, i.e. $\delta_0(\mathbf{k}) = \delta_L(\mathbf{k}; z = 0)$.

It often proves convenient to use $\eta = \ln D$ as a time variable, and to combine δ and θ into a two-component field

$$\Phi_a(\mathbf{k}) = \begin{pmatrix} \delta(\mathbf{k}) \\ -\theta(\mathbf{k})/\mathcal{H}f \end{pmatrix}. \quad (\text{A8})$$

If we introduce

$$\alpha(\mathbf{q}_1, \mathbf{q}_2) = \frac{\mathbf{k} \cdot \mathbf{q}_1}{q_1^2} \quad , \quad \beta(\mathbf{q}_1, \mathbf{q}_2) = \frac{k^2 (\mathbf{q}_1 \cdot \mathbf{q}_2)}{2q_1^2 q_2^2} \quad (\text{A9})$$

the fluid equations may be recast as

$$\left[\delta_{ab} \frac{\partial}{\partial \eta} + \Omega_{ab} \right] \Phi_b(\mathbf{k}; \eta) = \int \frac{d^3 q}{(2\pi)^3} \gamma_{abc}(\mathbf{q}, \mathbf{k} - \mathbf{q}) \Phi_b(\mathbf{q}; \eta) \Phi_c(\mathbf{k} - \mathbf{q}; \eta), \quad (\text{A10})$$

where

$$\Omega_{ab}(\eta) = \begin{pmatrix} 0 & -1 \\ -\frac{3\Omega_m}{2f^2} & \frac{3\Omega_m}{2f^2} - 1 \end{pmatrix} \quad (\text{A11})$$

and the vertex $\gamma_{abc}(\mathbf{q}_1, \mathbf{q}_2)$ only has nonzero entries $\gamma_{121}(\mathbf{q}_1, \mathbf{q}_2) = \gamma_{112}(\mathbf{q}_2, \mathbf{q}_1) = \alpha(\mathbf{q}_1, \mathbf{q}_2)/2$ and $\gamma_{222}(\mathbf{q}_1, \mathbf{q}_2) = \beta(\mathbf{q}_1, \mathbf{q}_2)$. The initial fields at time η_i are denoted

$$\phi_a(\mathbf{k}) \equiv \Phi_a(\mathbf{k}; \eta_i) = \delta_i(\mathbf{k}) \begin{pmatrix} 1 \\ 0 \end{pmatrix}, \quad (\text{A12})$$

and the linear theory solution is simply $\Phi_a^{(L)}(\mathbf{k}; \eta) = e^{\eta - \eta_i} \phi_a(\mathbf{k})$.

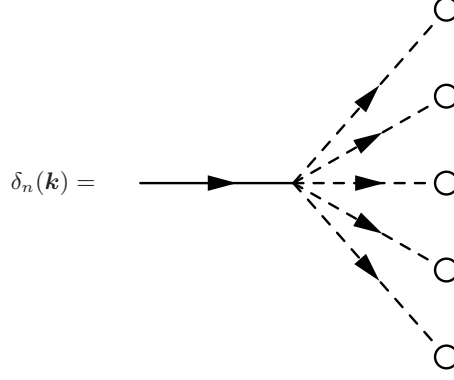


FIG. 9: Diagrammatic representation of the n^{th} order contribution to $\delta(\mathbf{k})$.

1. Beyond linear order

Standard perturbation theory (hereafter SPT; [16, 17, 18, 19, 20, 21]) defines a systematic series solution to the fluid equations (1) in powers of the initial density contrast δ_i (or equivalently in powers of the current linearly evolved density contrast δ_0). In an Einstein-de Sitter universe, where $\mathcal{H} \propto a^{-1/2}$ and $\Omega_m \mathcal{H}^2 \propto a^{-1}$, the expansion may be written as

$$\delta(\mathbf{k}; \tau) = \sum_{n=1}^{\infty} a^n(\tau) \delta_n(\mathbf{k}), \quad \theta(\mathbf{k}; \tau) = -\mathcal{H}(\tau) \sum_{n=1}^{\infty} a^n(\tau) \theta_n(\mathbf{k}), \quad (\text{A13})$$

where $\delta_n(\mathbf{k})$ and $\theta_n(\mathbf{k})$ are time-independent mode-coupling integrals over n powers of the initial density field:

$$\begin{pmatrix} \delta_n(\mathbf{k}) \\ \theta_n(\mathbf{k}) \end{pmatrix} = \int \frac{d^3 q_1 \dots d^3 q_n}{(2\pi)^{3n}} (2\pi)^3 \delta_D \left(\sum \mathbf{q}_i - \mathbf{k} \right) \begin{pmatrix} F_n(\{\mathbf{q}_i\}) \\ G_n(\{\mathbf{q}_i\}) \end{pmatrix} \delta_0(\mathbf{q}_1) \dots \delta_0(\mathbf{q}_n). \quad (\text{A14})$$

The kernels F_n and G_n satisfy recurrence relations that follow straightforwardly from the equations of motion [17, 18, 21]:

$$F_n(\mathbf{q}_1, \dots, \mathbf{q}_n) = \sum_{m=1}^{n-1} \frac{G_m(\mathbf{q}_1, \dots, \mathbf{q}_m)}{(2n+3)(n-1)} \left[(1+2n) \frac{\mathbf{k} \cdot \mathbf{k}_1}{k_1^2} F_{n-m}(\mathbf{q}_{m+1}, \dots, \mathbf{q}_n) + \frac{k^2(\mathbf{k}_1 \cdot \mathbf{k}_2)}{k_1^2 k_2^2} G_{n-m}(\mathbf{q}_{m+1}, \dots, \mathbf{q}_n) \right], \quad (\text{A15})$$

$$G_n(\mathbf{q}_1, \dots, \mathbf{q}_n) = \sum_{m=1}^{n-1} \frac{G_m(\mathbf{q}_1, \dots, \mathbf{q}_m)}{(2n+3)(n-1)} \left[3 \frac{\mathbf{k} \cdot \mathbf{k}_1}{k_1^2} F_{n-m}(\mathbf{q}_{m+1}, \dots, \mathbf{q}_n) + n \frac{k^2(\mathbf{k}_1 \cdot \mathbf{k}_2)}{k_1^2 k_2^2} G_{n-m}(\mathbf{q}_{m+1}, \dots, \mathbf{q}_n) \right], \quad (\text{A16})$$

where $\mathbf{k}_1 = \mathbf{q}_1 + \dots + \mathbf{q}_m$, $\mathbf{k}_2 = \mathbf{q}_{m+1} + \dots + \mathbf{q}_n$, $\mathbf{k} = \mathbf{k}_1 + \mathbf{k}_2$ and $F_1 = G_1 = 1$.

While the Einstein-de Sitter approximation is convenient, it is not necessary [47]. However we have confirmed that an accurate approximation is to substitute the growth factor $D(z)$ for a ,

$$\delta(\mathbf{k}; z) = \sum_{n=1}^{\infty} D^n(z) \delta_n(\mathbf{k}), \quad \theta(\mathbf{k}; z) = -\mathcal{H}f \sum_{n=1}^{\infty} D^n(z) \theta_n(\mathbf{k}), \quad (\text{A17})$$

with the same mode-coupling integrals as above for δ_n and θ_n . The validity of this approximation is ultimately traced to the fact that the ratio Ω_m/f^2 is very nearly unity over the entire lifetime of the universe for Λ CDM cosmologies, since $f \approx \Omega_m^{0.6}$ [12].

To compute statistical observables it is convenient to introduce diagrammatic rules for keeping track of the various terms in the perturbation series [17]. The function $\delta_n(\mathbf{k})$ (or $\theta_n(\mathbf{k})$) may be represented as in Figure 9, where the open circles denote factors of δ_0 , and the vertex denotes a momentum-conserving integral of F_n (or G_n) over intermediate wavevectors \mathbf{q}_i . Algebraically the n^{th} order contribution $P^{(n)}$ is obtained by isolating all terms of order $(\delta_0)^{2n}$ from

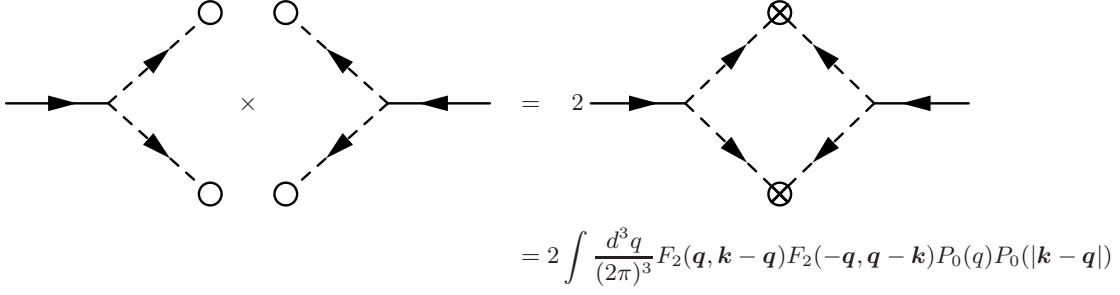


FIG. 10: Diagrammatic prescription for computing $P^{(2,2)}(k)$. The overall factor of 2 comes from the two equivalent ways of pairing the open circles. Only the single wavevector \mathbf{q} must be integrated over, the rest being determined by momentum conservation at vertices and translational invariance of the 2-point function.

the ensemble average $\langle \delta(\mathbf{k})\delta(\mathbf{k}') \rangle$, i.e.

$$(2\pi)^3 \delta_D(\mathbf{k} + \mathbf{k}') P^{(n)}(k; z) = D^{2n}(z) \sum_{m=1}^{2n-1} \langle \delta_m(\mathbf{k}) \delta_{2n-m}(\mathbf{k}') \rangle. \quad (\text{A18})$$

The quantity $\langle \delta_m(\mathbf{k}) \delta_{2n-m}(\mathbf{k}') \rangle$ may be represented diagrammatically by “multiplying” the diagrams for $\delta_m(\mathbf{k})$ and $\delta_{2n-m}(\mathbf{k}')$. Since the initial field δ_i (and hence δ_0) is Gaussian, ensemble averages of powers of δ_0 may be expanded in terms of the 2-point function P_0 according to Wick’s theorem. Then the product of the diagrams $\delta_m(\mathbf{k})$ and $\delta_{2n-m}(\mathbf{k}')$ is given by summing over all possible pairings of their open circles, where open circles are paired according to the rule

$$-\text{---}\blacktriangleright\text{---}\bigcirc \times \bigcirc \text{---}\blacktriangleleft\text{---} = -\text{---}\blacktriangleright\text{---}\bigotimes\text{---}\blacktriangleleft\text{---} \equiv (2\pi)^3 \delta_D(\mathbf{q} + \mathbf{q}') P_0(q), \quad (\text{A19})$$

with the additional understanding that any diagram containing a tadpole (a fragment connected to the rest of the diagram by a single edge) vanishes identically.

As an example we show in Figure 10 how to obtain the 2nd order contribution $P^{(2,2)}(k)$. Notice that after invoking momentum conservation at vertices and translational invariance of the 2-point function, only a single wavevector remains to be integrated. In general all diagrams contributing to $P^{(n)}$ contain $n - 1$ loops, requiring integration over $n - 1$ independent wavevectors. For this reason we often classify power spectrum terms by their number of loops rather than their “order,” which is a potentially ambiguous concept.

With this expansion, statistical observables may be computed straightforwardly in SPT to any fixed order. For example, the first correction to the matter power spectrum (second order in the initial power spectrum, fourth order in the initial density contrast, or 1-loop in the diagrammatic idiom) is given by

$$P(k) = P_L(k) + P^{(2,2)}(k) + P^{(1,3)}(k) \quad (\text{A20})$$

where $P_L(k; z) = D^2(z)P_0(k)$ is the linear power spectrum and [18]

$$P^{(1,3)}(k) = \frac{1}{252} \frac{k^3}{4\pi^2} P_L(k) \int_0^\infty dr P_L(kr) \left[\frac{12}{r^2} - 158 + 100r^2 - 42r^4 + \frac{3}{r^2} (r^2 - 1)^3 (7r^2 + 2) \ln \left| \frac{1+r}{1-r} \right| \right], \quad (\text{A21a})$$

$$P^{(2,2)}(k) = \frac{1}{98} \frac{k^3}{4\pi^2} \int_0^\infty dr P_L(kr) \int_{-1}^1 dx P_L \left(k \sqrt{1+r^2-2rx} \right) \frac{(3r+7x-10rx^2)^2}{(1+r^2-2rx)^2}. \quad (\text{A21b})$$

At low k , $P^{(2,2)}$ is positive while $P^{(1,3)}$ is negative, and there is a large degree of cancellation between them. For large k

$$P^{(2,2)}(k) \sim \frac{1}{4} \Sigma^2 k^2 P_L(k) \quad \text{and} \quad P^{(1,3)}(k) \sim -\frac{1}{2} \Sigma^2 k^2 P_L(k) \quad (\text{A22})$$

where Σ is defined by Eq. (7), so for sufficiently large k the total second order contribution is negative.

It is also straightforward to derive expressions for the velocity power spectrum [18]

$$P_{\theta\theta}^{(1,3)}(k) = \frac{1}{84} \frac{k^3}{4\pi^2} P_L(k) \int_0^\infty dr P_L(kr) \left[\frac{12}{r^2} - 82 + 4r^2 - 6r^4 + \frac{3}{r^2} (r^2 - 1)^3 (r^2 + 2) \ln \left| \frac{1+r}{1-r} \right| \right], \quad (\text{A23})$$

$$P_{\theta\theta}^{(2,2)}(k) = \frac{1}{98} \frac{k^3}{4\pi^2} \int_0^\infty dr P_L(kr) \int_{-1}^1 dx P_L \left(k \sqrt{1+r^2-2rx} \right) \frac{(7x-r-6rx^2)^2}{(1+r^2-2rx)^2}. \quad (\text{A24})$$

the density-velocity cross-spectrum (e.g. [48])

$$P_{\delta\theta}^{(1,3)}(k) = \frac{1}{252} \frac{k^3}{4\pi^2} P_L(k) \int_0^\infty dr P_L(kr) \left[\frac{24}{r^2} - 202 + 56r^2 - 30r^4 + \frac{3}{r^2} (r^2 - 1)^3 (5r^2 + 4) \ln \left| \frac{1+r}{1-r} \right| \right], \quad (\text{A25})$$

$$P_{\delta\theta}^{(2,2)}(k) = \frac{1}{98} \frac{k^3}{4\pi^2} \int_0^\infty dr P_L(kr) \int_{-1}^1 dx P_L(k\sqrt{1+r^2-2rx}) \frac{(3r+7x-10rx^2)(7x-r-6rx^2)}{(1+r^2-2rx)^2}, \quad (\text{A26})$$

and the propagator

$$G(k) \simeq 1 + \frac{P^{(1,3)} + P^{(1,5)} + \dots}{2P_L}. \quad (\text{A27})$$

Though it is not usually considered, there is no real obstacle in going to the next order in the systematic perturbative expansion described above. For the third order (2-loop) contribution one finds $P^{(3)}(k) = P^{(1,5)}(k) + P^{(2,4)}(k) + P^{(3,3)}(k)$ with [42]

$$P^{(1,5)}(k) = 30P_L(k) \int \frac{d^3q}{(2\pi)^3} \frac{d^3p}{(2\pi)^3} F_5^{(s)}(\mathbf{k}, \mathbf{q}, -\mathbf{q}, \mathbf{p}, -\mathbf{p}) P_L(q) P_L(p) \quad (\text{A28})$$

$$P^{(2,4)}(k) = 24 \int \frac{d^3q}{(2\pi)^3} \frac{d^3p}{(2\pi)^3} F_2^{(s)}(\mathbf{q}, \mathbf{k} - \mathbf{q}) F_4^{(s)}(-\mathbf{q}, \mathbf{q} - \mathbf{k}, \mathbf{p}, -\mathbf{p}) P_L(q) P_L(p) P_L(|\mathbf{k} - \mathbf{q}|) \quad (\text{A29})$$

$$P^{(3,3)}(k) = \int \frac{d^3q}{(2\pi)^3} \frac{d^3p}{(2\pi)^3} \left[9F_3^{(s)}(\mathbf{q}, -\mathbf{q}, \mathbf{k}) F_3^{(s)}(-\mathbf{k}, \mathbf{p}, -\mathbf{p}) P_L(k) P_L(q) P_L(p) \right. \\ \left. + 6F_3(\mathbf{q}, \mathbf{p}, \mathbf{k} - \mathbf{q} - \mathbf{p}) F_3(-\mathbf{q}, -\mathbf{p}, \mathbf{q} + \mathbf{p} - \mathbf{k}) P_L(q) P_L(p) P_L(|\mathbf{k} - \mathbf{q} - \mathbf{p}|) \right] \quad (\text{A30})$$

and with $F_n^{(s)}$ given by Eq. (A15) symmetrized over its n arguments $\mathbf{q}_1, \dots, \mathbf{q}_n$. Using rotational symmetry to eliminate one azimuthal integration, the resulting expressions require 5-dimensional mode-coupling integrals which are best performed using Monte Carlo methods.

Expressions for higher order contributions are not difficult to derive, but the computational costs of evaluating them quickly spiral out of control. In general the ℓ -loop contribution requires mode-coupling integrals of dimension 3ℓ ($3\ell - 1$ after rotational symmetry), making 1-loop simple, 2-loop possible, and higher orders impracticable.

APPENDIX B: LAGRANGIAN PERTURBATION THEORY

The Lagrangian description of structure formation [49, 50, 51] relates the current, or Eulerian, position of a mass element, \mathbf{x} , to its initial, or Lagrangian, position, \mathbf{q} , through a displacement vector field: $\mathbf{x} = \mathbf{q} + \Psi(\mathbf{q})$. (Note that \mathbf{q} is used as a position vector in the Lagrangian picture, whereas the same symbol is used as a wavevector in the Eulerian picture.) The displacements can be related to overdensities by [52]

$$\delta(\mathbf{x}) = \int d^3q \delta_D(\mathbf{x} - \mathbf{q} - \Psi) - 1 \quad , \quad \delta(\mathbf{k}) = \int d^3q e^{-i\mathbf{k}\cdot\mathbf{q}} \left(e^{-i\mathbf{k}\cdot\Psi(\mathbf{q})} - 1 \right). \quad (\text{B1})$$

The displacements evolve according to

$$\frac{d^2\Psi}{dt^2} + 2H \frac{d\Psi}{dt} = -\nabla_x \phi[\mathbf{q} + \Psi(\mathbf{q})], \quad (\text{B2})$$

where here and only here ϕ is the gravitational potential. Analogous to Eulerian perturbation theory, standard LPT expands the displacement in powers of the linear density field with [53]

$$\Psi^{(n)}(\mathbf{k}) = \frac{i}{n!} \int \prod_{i=1}^n \left[\frac{d^3k_i}{(2\pi)^3} \right] (2\pi)^3 \delta_D \left(\sum_i \mathbf{k}_i - \mathbf{k} \right) \mathbf{L}^{(n)}(\mathbf{k}_1, \dots, \mathbf{k}_n, \mathbf{k}) \delta_0(\mathbf{k}_1) \dots \delta_0(\mathbf{k}_n). \quad (\text{B3})$$

and the $\mathbf{L}^{(n)}$ have closed form expressions in terms of dot products of wave vectors which can be generated by recurrence relations. Expanding the exponential in Eq. (B1) we obtain a perturbative series for the overdensity, $\delta = \delta^{(1)} + \delta^{(2)} + \dots$ where, e.g.,

$$\delta^{(2)}(\mathbf{k}) = \frac{1}{2} \int \frac{d^3k_1 d^3k_2}{(2\pi)^3} \delta_D(\mathbf{k}_1 + \mathbf{k}_2 - \mathbf{k}) \delta_0(\mathbf{k}_1) \delta_0(\mathbf{k}_2) \left[\mathbf{k} \cdot \mathbf{L}^{(2)}(\mathbf{k}_1, \mathbf{k}_2, \mathbf{k}) + \mathbf{k} \cdot \mathbf{L}^{(1)}(\mathbf{k}_1) \mathbf{k} \cdot \mathbf{L}^{(1)}(\mathbf{k}_2) \right] \quad (\text{B4})$$

is second order in the linear density field δ_0 .

A similar expansion can be performed for the power spectrum, which from Eq. (B1) can be written

$$P(k) = \int d^3q e^{-i\mathbf{k}\cdot\mathbf{q}} (\langle e^{-i\mathbf{k}\cdot\Delta\Psi} \rangle - 1) \quad (\text{B5})$$

where $\Delta\Psi = \Psi(\mathbf{q}) - \Psi(0)$ and we have used translational invariance.

Alternatively [31] suggested using the cumulant expansion theorem for the exponential in Eq. (B5) and using the binomial theorem to expand the term $(\mathbf{k}\cdot\Delta\Psi)^N$. One obtains two types of terms: those depending on Ψ at the same point and those depending on Ψ at two different points. Owing to statistical homogeneity the first type of term is independent of position and can be factored out of the integral leaving [31]

$$P(k) = \exp \left[-2 \sum_{n=1}^{\infty} (-1)^{n-1} \langle [\mathbf{k}\cdot\Psi(0)]^{2n} \rangle \right] \int d^3r e^{i\mathbf{k}\cdot\mathbf{r}} \left\{ \exp \left[\sum_{N=2}^{\infty} \frac{k_{i_1} \dots k_{i_N}}{N!} B_{i_1 \dots i_N}^{(N)}(\mathbf{r}) \right] - 1 \right\}, \quad (\text{B6})$$

where $k_{i_1} \dots k_{i_N} B_{i_1 \dots i_N}^{(N)}(\mathbf{r})$ is shorthand for the second type of term.

In a traditional perturbative calculation one would expand this expression to a fixed order in Ψ ; this approach indeed reproduces the SPT result to 2nd order. However one might expect that the position-independent cumulant factors are more important on large scales than the position-dependent ones, suggesting that these factors should be left unexpanded in the exponential. Using well-known previous results from LPT the first corrections to the power spectrum are then [31]

$$P(k) = e^{-(k\Sigma)^2/2} \left[P_L(k) + P^{(2,2)}(k) + \tilde{P}^{(1,3)}(k) \right], \quad (\text{B7})$$

where Σ is given by Eq. (7), $P^{(2,2)}(k)$ is as in SPT [Eq. (A21b)] and

$$\tilde{P}^{(1,3)}(k) = \frac{1}{252} \frac{k^3}{4\pi^2} P_L(k) \int_0^\infty dr P_L(kr) \left[\frac{12}{r^2} + 10 + 100r^2 - 42r^4 + \frac{3}{r^3} (r^2 - 1)^3 (7r^2 + 2) \ln \left| \frac{1+r}{1-r} \right| \right]. \quad (\text{B8})$$

Notice that this differs from the SPT result [Eq. (A21a)] only by the replacement $-158 \rightarrow 10$ in the brackets. If the exponential prefactor is expanded to first order in P_L the SPT result is recovered exactly [31]. Also note that the first term $e^{-\Sigma^2 k^2/2} P_L(k)$ is identical to the tree-level RPT result in the large- k limit.

-
- [1] D. J. Eisenstein, *New Astronomy Review* **49**, 360 (2005).
 - [2] A. Taruya and T. Hiramatsu, *Astrophys. J.* **674**, 617 (2008), 0708.1367.
 - [3] T. Nishimichi, A. Shirata, A. Taruya, K. Yahata, S. Saito, Y. Suto, R. Takahashi, N. Yoshida, T. Matsubara, N. Sugiyama, et al., *ArXiv e-prints* (2008), 0810.0813.
 - [4] P. Valageas, *Astron. Astrophys.* **484**, 79 (2008), 0711.3407.
 - [5] F. Bernardeau, M. Crocce, and R. Scoccimarro, *Phys. Rev. D* **78**, 103521 (2008), 0806.2334.
 - [6] H. Guo and Y. P. Jing, *ArXiv e-prints* (2009), 0904.3200.
 - [7] K. Heitmann, M. White, C. Wagner, S. Habib, and D. Higdon, *ArXiv e-prints* (2008), 0812.1052.
 - [8] K. Heitmann, Z. Lukić, P. Fasel, S. Habib, M. S. Warren, M. White, J. Ahrens, L. Ankeny, R. Armstrong, B. O'Shea, et al., *Computational Science and Discovery* **1**, 015003 (2008), 0706.1270.
 - [9] A. E. Evrard, J. Bialek, M. Busha, M. White, S. Habib, K. Heitmann, M. Warren, E. Rasia, G. Tormen, L. Moscardini, et al., *Astrophys. J.* **672**, 122 (2008), arXiv:astro-ph/0702241.
 - [10] G. Hinshaw, J. L. Weiland, R. S. Hill, N. Odegard, D. Larson, C. L. Bennett, J. Dunkley, B. Gold, M. R. Greason, N. Jarosik, et al., *ArXiv e-prints* (2008), 0803.0732.
 - [11] A. Slosar, C. Hirata, U. Seljak, S. Ho, and N. Padmanabhan, *Journal of Cosmology and Astro-Particle Physics* **8**, 31 (2008), 0805.3580.
 - [12] F. Bernardeau, S. Colombi, E. Gaztañaga, and R. Scoccimarro, *Phys. Rep.* **367**, 1 (2002), arXiv:astro-ph/0112551.
 - [13] M. Crocce and R. Scoccimarro, *Phys. Rev. D* **73**, 063519 (2006), arXiv:astro-ph/0509418.
 - [14] M. Crocce and R. Scoccimarro, *Phys. Rev. D* **73**, 063520 (2006), arXiv:astro-ph/0509419.
 - [15] V. L'vov and I. Procaccia, *Exact resummations in the theory of hydrodynamic turbulence: 0. line-resummed diagrammatic perturbation approach* (1995), URL <http://www.citebase.org/abstract?id=oai:arXiv.org:chao-dyn/9502010>.
 - [16] E. T. Vishniac, *Mon. Not. R. Astron. Soc.* **203**, 345 (1983).
 - [17] M. H. Goroff, B. Grinstein, S.-J. Rey, and M. B. Wise, *Astrophys. J.* **311**, 6 (1986).
 - [18] N. Makino, M. Sasaki, and Y. Suto, *Phys. Rev. D* **46**, 585 (1992).

- [19] P. J. E. Peebles, *The large-scale structure of the universe* (Princeton University Press, Princeton, NJ, 1980).
- [20] R. Juszkiewicz, *Mon. Not. R. Astron. Soc.* **197**, 931 (1981).
- [21] B. Jain and E. Bertschinger, *Astrophys. J.* **431**, 495 (1994), arXiv:astro-ph/9311070.
- [22] M. Crocce and R. Scoccimarro, *Phys. Rev. D* **77**, 023533 (2008), 0704.2783.
- [23] H. W. Wyld, Jr., *Annals of Physics* **14**, 143 (1961).
- [24] M. Pietroni, *Journal of Cosmology and Astro-Particle Physics* **10**, 36 (2008), 0806.0971.
- [25] J. Lesgourgues, S. Matarrese, M. Pietroni, and A. Riotto, *ArXiv e-prints* (2009), 0901.4550.
- [26] P. McDonald, *Phys. Rev. D* **75**, 043514 (2007), arXiv:astro-ph/0606028.
- [27] P. Valageas, *Astron. Astrophys.* **379**, 8 (2001), arXiv:astro-ph/0107015.
- [28] P. Valageas, *Astron. Astrophys.* **382**, 412 (2002), arXiv:astro-ph/0107126.
- [29] P. Valageas, *Astron. Astrophys.* **421**, 23 (2004), arXiv:astro-ph/0307008.
- [30] P. Valageas, *Astron. Astrophys.* **465**, 725 (2007), arXiv:astro-ph/0611849.
- [31] T. Matsubara, *Phys. Rev. D* **77**, 063530 (2008), 0711.2521.
- [32] T. Matsubara, *Phys. Rev. D* **78**, 083519 (2008), 0807.1733.
- [33] T. Buchert, *Mon. Not. R. Astron. Soc.* **254**, 729 (1992).
- [34] T. Buchert and J. Ehlers, *Mon. Not. R. Astron. Soc.* **264**, 375 (1993).
- [35] T. Buchert, *Mon. Not. R. Astron. Soc.* **267**, 811 (1994), arXiv:astro-ph/9309055.
- [36] M. White, *ApJS* **143**, 241 (2002), arXiv:astro-ph/0207185.
- [37] V. Springel, *Mon. Not. R. Astron. Soc.* **364**, 1105 (2005), arXiv:astro-ph/0505010.
- [38] R. W. Hockney and J. W. Eastwood, *Computer simulation using particles* (Bristol: Hilger, 1988).
- [39] M. White, Y.-S. Song, and W. J. Percival, *ArXiv e-prints* (2008), 0810.1518.
- [40] D. J. Eisenstein and W. Hu, *Astrophys. J.* **496**, 605 (1998), arXiv:astro-ph/9709112.
- [41] D. Jeong and E. Komatsu, *Astrophys. J.* **651**, 619 (2006), arXiv:astro-ph/0604075.
- [42] J. N. Fry, *Astrophys. J.* **421**, 21 (1994).
- [43] E. Sefusatti and E. Komatsu, *Phys. Rev. D* **76**, 083004 (2007), 0705.0343.
- [44] T. Hiramatsu and A. Taruya, *ArXiv e-prints* (2009), 0902.3772.
- [45] W. J. Percival and M. White, *ArXiv e-prints* (2008), 0808.0003.
- [46] S. Pueblas and R. Scoccimarro, *ArXiv e-prints* (2008), 0809.4606.
- [47] R. Takahashi, *Progress of Theoretical Physics* **120**, 549 (2008), 0806.1437.
- [48] R. Scoccimarro, *Phys. Rev. D* **70**, 083007 (2004), arXiv:astro-ph/0407214.
- [49] T. Buchert, *Astron. Astrophys.* **223**, 9 (1989).
- [50] F. Moutarde, J.-M. Alimi, F. R. Bouchet, R. Pellat, and A. Ramani, *Astrophys. J.* **382**, 377 (1991).
- [51] E. Hivon, F. R. Bouchet, S. Colombi, and R. Juszkiewicz, *Astron. Astrophys.* **298**, 643 (1995), arXiv:astro-ph/9407049.
- [52] A. N. Taylor and A. J. S. Hamilton, *Mon. Not. R. Astron. Soc.* **282**, 767 (1996), arXiv:astro-ph/9604020.
- [53] F. R. Bouchet, S. Colombi, E. Hivon, and R. Juszkiewicz, *Astron. Astrophys.* **296**, 575 (1995), arXiv:astro-ph/9406013.
- [54] We bin the model into the same finite-width bins as the N-body data when making the comparison to the latter.